Self-shading of two-axis tracking solar collectors

Impact of field layout, latitude, and aperture shape

Jensen, Adam R.; Sifnaios, Ioannis; Furbo, Simon; Dragsted, Janne

Published in:
Solar Energy

Link to article, DOI:
10.1016/j.solener.2022.02.023

Publication date:
2022

Document Version
Publisher's PDF, also known as Version of record

Solar Energy 236 (2022) 215–224

Contents lists available at ScienceDirect

Solar Energy

journal homepage: www.elsevier.com/locate/solener

Self-shading of two-axis tracking solar collectors: Impact of field layout, latitude, and aperture shape

Adam R. Jensen *, Ioannis Sifnaios, Simon Furbo, Janne Dragsted

Department of Civil Engineering, Technical University of Denmark, Brovej, Building 118, Kgs. Lyngby 2800, Denmark

ARTICLE INFO

Keywords:
Sun-pointing
Sun-tracking
Dual-axis tracking
Mutual shading
Solar thermal collector
Photovoltaic (PV)

ABSTRACT

In this paper, an open source method for calculating self-shading in fields of two-axis tracking solar collectors of arbitrary geometry was developed and validated. The method was used to investigate the impact of latitude and collector aperture shape on annual shading loss. Simulations were carried out for the entire design space of field layouts by uniformly discretizing the layout parameters, i.e., aspect ratio, offset, rotation, and ground cover ratio. Results showed shading losses generally increase with latitude, and the optimum aspect ratio decreases with distance from the equator. Aperture shape was shown to significantly impact power output; the annual shading loss was lowest for the rectangular collector and highest for the square collector. Also, the impact of sub-optimal rotation of rectangular arrays was presented.

1. Introduction

To maximize the incident solar irradiation and reduce incidence angle losses, solar collectors and panels can be mounted on solar trackers. Solar trackers continuously optimize their orientation throughout the day and can generally be classified as either one-axis or two-axis trackers (Nsengiyumva et al., 2018). One-axis trackers rotate around a single axis, usually oriented north-south since this configuration results in the greatest annual energy yield (Tian et al., 2018). Employing two-axis trackers further increases the incident irradiation, as they maintain the collector surface normal to the sun and thus eliminate incidence angle losses. Therefore, two-axis trackers are particularly suitable for highly concentrating solar energy technologies, such as parabolic dish concentrators, Fresnel lens solar collectors, and concentrating photovoltaics (PV) (Duffie et al., 2020).

While two-axis tracking results in greater annual energy yields, accounting for self-shading is imperative as the relative shading losses are often considerably higher for two-axis trackers than fixed-tilt collectors (Gordon and Wenger, 1991). Self-shading occurs when one or more collectors block part of the irradiance on another collector. The extent of self-shading can be reduced by increasing the distance between collectors, though resulting in increased occupied land area. Land occupation is quantified by the ground cover ratio (GCR), defined as the ratio between the total collector area and the total field area (Narvarte and Lorenzo, 2008). While a system with a lower GCR experiences less shading and thus has a greater energy yield, this comes at the expense of greater investment requirements due to increased land procurement and longer connecting cables/pipes.

The annual impact of self-shading in two-axis tracking collector fields depends on the collector arrangement, henceforth referred to as field layout. For a fixed GCR, it is possible to minimize self-shading by choosing a favorable field layout. Determining the impact of different collector arrangements on shading involves simulating shading losses for a range of regularly spaced field layouts. The optimal field layout, i.e., that which minimizes shading losses for a given GCR, can then be determined (Cumpston and Pye, 2014).

Several previous studies have investigated the impact of two-axis tracking collector field layouts on shading. Apley (1979), for example, determined the optimal aspect ratio for trackers with circular apertures by calculating the annual shading losses of rectangular field layouts with a GCR of 0.196. The study found that shading was reduced when the E-W spacing between collectors was slightly greater than the N-S spacing. This is due to an increased distance between collectors during the early morning and late afternoon when shading is most pronounced.

Pons and Dugan (1984) and Meller (2010) expanded the study of Apley (1979) by investigating rectangular field layouts for GCRs between 0.2 and 0.785. Both studies presented results for the optimal N-S and E-W spacing and found that the optimum aspect ratio decreases with increasing GCR.

Practically all studies on shading of two-axis tracking collectors

* Corresponding author.
E-mail address: arajen@dtu.dk (A.R. Jensen).

https://doi.org/10.1016/j.solener.2022.02.023
Received 1 September 2021; Received in revised form 26 January 2022; Accepted 12 February 2022
Available online 9 March 2022

investigate only a small sub-set of possible field layouts (e.g., square or rectangular field layouts). One noticeable exception is the study by Cumpston and Pye (2014), which investigated the entire range of possible field layouts for GCRs between 0.1 and 0.9 for circular apertures. The study found that rectangular layouts were optimal for GCRs below 0.23. Whereas for GCRs greater than 0.23, diamond layouts of varying aspect ratios minimized shading. Preliminary results showed that a similar trend might exist for square apertures, though the study recommended more detailed investigations into optimum layouts for different aperture shapes.

So far, rectangular apertures have only been investigated in studies focused on PV, e.g., Díaz-Dorado et al. (2017). However, PV panels are affected by mismatch losses, hence the resulting power reduction is greater than the irradiance loss. Results from PV shading studies are therefore not directly transferrable to other technologies or even different module layouts. For the sake of generality, this study focuses only on irradiance losses due to shading and does not investigate the impact on specific technologies.

Furthermore, while optimal layouts have been frequently investigated, studies have mainly focused on sites in the sun-belt region (lat.: 25-36°), neglecting the potential differences in shading at higher latitudes. In recent years, however, Northern Europe has seen an increasing number of concentrating solar collector plants. Most recently, a plant of 144 two-axis tracking Fresnel lens solar collectors was constructed in 2019 in Lendemarke, Denmark (lat.: 55.0° N) (Jensen, 2022). At the time of writing, another two-axis tracking collector field was under construction in Hørsholm, Denmark (lat.: 55.9° N). Despite the influx of two-axis trackers at northern latitudes, no study has yet investigated self-shading of two-axis tracking collectors at latitudes higher than 45° N.

Another factor impacting self-shading is the collector aperture geometry. To date, studies concerning optimum layouts have focused on circular and square aperture geometries (Meller, 2010). At present, however, two-axis trackers typically feature rectangular apertures. A primary motivation for designing rectangular collectors over square collectors is that rectangular apertures can support larger aperture areas for the same support structure.

Furthermore, studies on two-axis tracker shading have most often used irradiance data from Barstow, California, from 1976. The dataset has a 15-min resolution and is freely available from NREL at nrel.gov/grid/solar-resource/west.html. Apley (1979) was the first to use this dataset, which has since been adopted as the de facto standard for shading calculation studies (e.g., Cumpston and Pye, 2014; Meller, 2010; Pons and Dugan, 1984; Osborn, 1980), despite the availability of more recent and higher resolution datasets.

To compare the energy yield for different field layouts, it is necessary to be able to determine the amount of self-shading at any given time. This can be accomplished with several different methods, including ray-tracing, which simulates the interaction of a large number of rays through an optical system (Fartaria and Pereira, 2013). While ray-tracing can generate very accurate results, it is too computationally expensive for optimization and engineering studies that require fast simulation times. To this end, Apley (1979) developed the SHADE algorithm, which approximates the collector surface as a grid of discrete points and calculates the shading fraction as the sum of shaded points divided by the total number of points. However, the accuracy of such numerical methods depends on the number of points used; hence, Linn and Zimmerman (1979) developed an analytical method suitable for circular and rectangular apertures. Their method relies on identifying several cases of overlapping shading, where the shaded area is calculated using an algorithm for the specific case. Due to the limited number of overlapping shading cases defined, the method is only able to consider shading contributions of the immediate surrounding collectors.

Several similar methods have been developed for determining blocking losses in heliostat fields caused by neighboring heliostats. Noone et al. (2012) developed a model based on a discretization of the curved heliostat mirror surfaces (similar approach as the SHADE algorithm), whereas Elayeb et al. (2014) presented an analytical and iterative method.

To overcome the geometry limitations of existing numerical methods for two-axis tracker shading, Meller (2010) presented a generic analytical method suitable for both convex and concave apertures. Nevertheless, this method was only implemented for circular collectors, and the source code was not disclosed. Moreover, most common solar energy simulation programs (e.g., SAM (Gilman et al., 2017), PVWatts (Dobos, 2014), TRNSYS (Klein et al., 2017)) lack the capability to simulate shading of two-axis tracking systems.

As is evident, the current literature does not sufficiently cover the impact of higher latitudes (>45° N) and has narrowly focused on circular and square apertures. This study seeks to address these topics. Thus, the novelty of this paper can be categorized into two primary areas: (1) determining the impact of aperture shape by comparing shading results for a circular, a square, and a rectangular aperture, and (2) determining the influence of latitude by comparing differences in shading at four different locations.

The outline of this paper is as follows: first, the three aperture shapes are defined in Section 2.1, and the discrete collector field layouts are introduced in Section 2.2. Next, a shading method that is suitable for simulating any geometry aperture shape and field layout is described in Section 2.3. The annual shading loss metric is introduced in Section 2.4, and the four different locations are described in Section 2.5, followed by a definition of the reference scenario in Section 2.6.

The results of the simulations and accompanying discussions are presented in Section 3. The shading method is validated in Section 3.1, and the model outputs are presented in Section 3.2. The optimum field layouts and the influence of field layout parameters are presented in Sections 3.3 and 3.4, respectively. This is followed by an analysis of rectangular field layouts in Section 3.5. Lastly, a conclusion of the study is given in Section 4.

2. Methods

This section describes the discrete field layouts and the method used for calculating self-shading of two-axis tracking collectors. The shading method consists of three main parts: definition of collector aperture geometry, generation of field layouts, and calculation of the shading fraction. The section ends with a brief description of the annual shading loss, investigated locations, irradiance data, and reference scenario.

2.1. Aperture geometries

The collector aperture geometry is defined as a polygon corresponding to the outer edges of the collector aperture. The polygon vertices are specified with respect to the origin, which represents the center of rotation. The shading calculations described in Section 2.3 can be used for any aperture geometry, including concave polygons and circular apertures (approximated as 64-sided polygons).

The aperture geometry dictates the maximum feasible GCR (GCR_{max}), which is achieved when neighboring collectors are able to touch each other. Under the constraint that collectors should be able to freely rotate without colliding, the minimum distance between two collectors, D_{min}, is equal to the diameter of the minimum bounding circle of the collector aperture. As an example, for circular collectors rotating around the center, D_{min} is equal to the diameter, and GCR_{max} is 0.91.

The influence of aperture shape was examined by comparing the optimal field layouts for circular, square, and rectangular apertures. The investigated rectangular aperture had an aspect ratio of 1.85, i.e., a collector width 1.85 times the height. For the rectangular aperture, GCR_{max} is 0.48, which is considerably lower than for circular apertures, as collectors with rectangular apertures cannot be arranged as close. The absolute dimensions of the collector aperture can be chosen arbitrarily, as the GCR scales the field layout according to the collector area.

2.2. Collector field layouts

This study examines regular field layouts, i.e., field layouts where the arrangement of immediate neighbors is the same for all collectors. Following the methodology of Cumpston and Pye (2014), regular field layouts can be fully defined by four parameters:

1. Aspect ratio: The ratio of the distance between collector columns to the distance between collector rows.
2. Offset: Relative offset of adjacent columns of collectors as a fraction of the distance between rows.
3. Rotation: Rotation of the collector field in the counterclockwise direction.
4. Ground cover ratio (GCR): Ratio of the collector area (A_{col}) to the field area occupied by each collector.

The effect of each parameter is demonstrated graphically in Fig. 1, where each parameter is applied in succession, ending with a fully defined layout.

2.2.1. Layout discretization

To find the optimal field layout, a numerical search of the entire parameter space of layouts has been completed, i.e., investigating the complete range of aspect ratios, offsets, and rotations for the GCRs of interest.

This study opts for a uniform discretization of the design space. This method allows for a more transparent comparison than alternative methods, such as recursive incrementation used by Cumpston and Pye (2014). The simulated layouts cover the entire design space of aspect ratios, rotations, and offsets, ranging from the minimum to the maximum feasible values using a constant step size (for a derivation of parameter limits, see Cumpston and Pye (2014)).

The range and step size of the discrete values for each parameter are listed in Table 1. To illustrate the layout discretization, the discrete aspect ratios and offsets for the rectangular aperture are shown in Fig. 2 for GCRs of 0.2 and 0.3. The discretization resulted in a total of $3.72{\cdot}10^6$, $1.75{\cdot}10^6$, and $1.27{\cdot}10^6$ unique collector field layouts for the circular, square, and rectangular aperture, respectively.

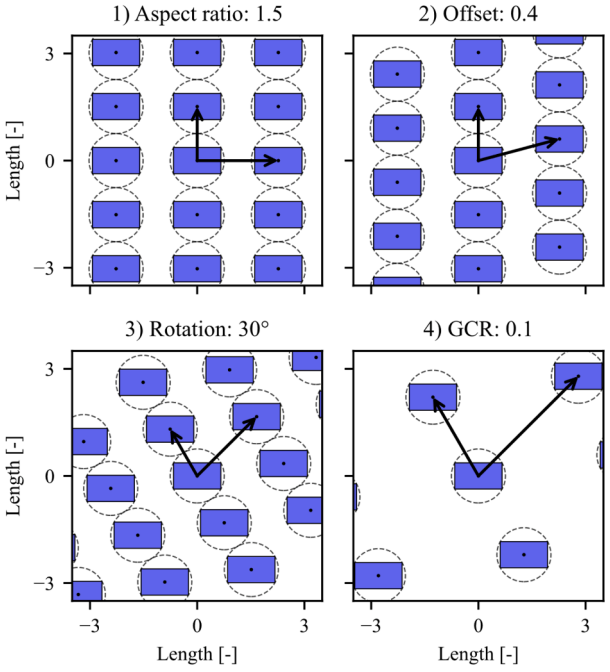

Fig. 1. Graphical illustration of the four-step process defining regularly spaced collector field layouts. The minimum distance between collectors, D_{min}, is represented by the dashed circle around each collector.

Table 1
Discretization of field layout simulations. Range and step size for each of the four defining parameters of regular field layouts. Square brackets denote a closed interval, i.e., the inclusion of endpoints.

Parameter	Range and step size
Offset	[−0.5, 0.5] in steps of 0.05
Rotation	[0°, 180°) in steps of 5°
GCR	[0.1, GCR_{max}] in steps of 0.05
Aspect ratio	$[\sqrt{1-\text{offset}^2}, A_{col}/(GCR{\cdot}D_{min}{}^2)]$ for values evenly divisible by 0.05

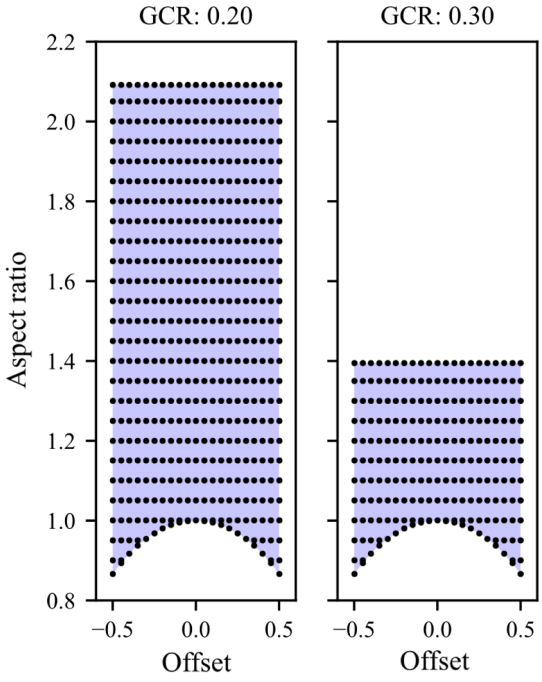

Fig. 2. Illustration of the discrete aspect ratio and offset simulation values for GCR 0.2 and 0.3 for the rectangular aperture. Each point represents a unique combination of aspect ratio, GCR, and offset, which is simulated for 36 different rotations. The blue area represents the feasible design space for the specified GCR.

2.2.2. Edge-effects

Collectors on the perimeter of a collector field experience less shading than collectors located within the field, as illustrated in Fig. 3. Such field-edge effects are often neglected, and shading is calculated for

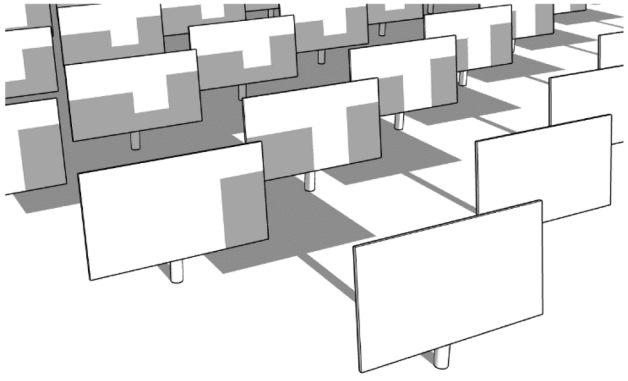

Fig. 3. Self-shading of two-axis tracking collectors in a collector field. The illustration demonstrates how edge collectors experience less shading than collectors within the field.

one reference collector within the field, as intra-field collectors experience similar shading conditions. While this simplification potentially results in the overestimation of shading losses, it has previously been demonstrated that edge effects are negligible for fields with more than 50 collectors (Pons and Dugan, 1984).

2.2.3. Neighbor order

Once it has been established that it is sufficient to calculate shading for a reference collector, it is necessary to determine which neighboring collectors should be considered in the shading calculations. This can be accomplished using neighbor order. For a neighbor order of one, only the immediate eight neighboring collectors are considered. A neighbor order of two additionally includes the collectors adjacent to the first-order neighbors, increasing the total number of considered collectors to 24.

Simulation times increase dramatically with increasing neighbor order, leading most studies to only consider first-order neighbors (e.g., Linn and Zimmerman, 1979; Meller and Kribus, 2013). Meller (2010) investigated the impact of including first vs. second-order neighbors for a square field layout at two different locations. The study found no difference in the annual shading loss at the southern location (lat.: 32° N). However, for the northern location (lat.: 41° N), using only first-order neighbors underestimated the annual shading loss by up to 1.7%. This indicates that higher-order neighbors may be more important at higher latitudes; thus, in this study, a neighbor order of two is used.

2.3. Shading calculation

The shading calculation method is analytical and consists of three steps: projecting shadows of neighboring collectors onto the reference collector plane, selecting collectors that potentially contribute to shading, and calculating the shaded area of the reference collector.

This procedure must be carried out for each time-step, as shading conditions continuously change with changing sun position and tracker orientation. The sun position is defined by the solar elevation angle, α, and azimuth angle, γ (measured clockwise from north), as shown in Fig. 4. For two-axis trackers, the collector tilt is equal to the complement of the solar elevation angle, and the collector azimuth is the same as the solar azimuth.

2.3.1. Projection of shadows onto the reference plane

The first step to determine shading by a neighboring collector is to project the shadow cast by the neighboring collector onto the plane of the reference collector. As all collector surfaces point toward the sun, their aperture planes are parallel, causing the shadow cast by a neighboring collector to have the same geometry and size as the reference collector.

The projected shadow can therefore be defined by the offsets in the x- and y-directions (x_0 and y_0) relative to the reference collector. The x-direction is parallel to the ground, and the y-direction is orthogonal to the x-direction. An example of the shadow projection is shown in Fig. 5, exemplifying the projection of the shadow cast by the shading collector in Fig. 4.

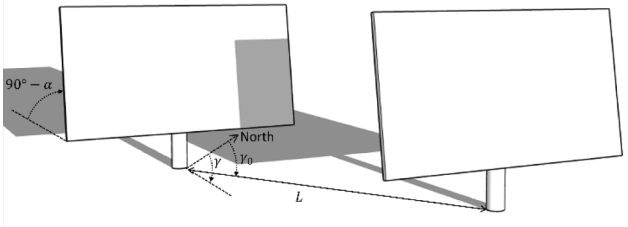

Fig. 4. Schematic of the reference collector being shaded by a neighboring collector.

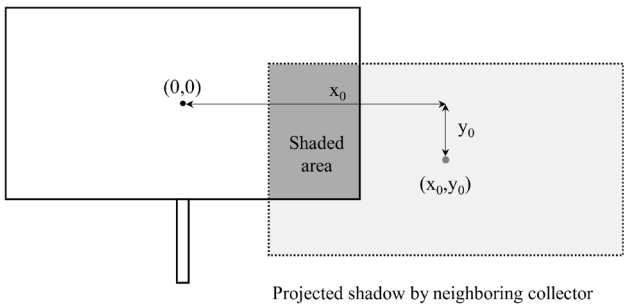

Fig. 5. Projection of the shadow cast by a neighboring collector onto the reference collector plane. Orthogonal view of the reference collector plane.

The offsets of the projected shadow can be calculated geometrically based on the field layout and sun position. To simplify the geometric calculations, the locations of neighboring collectors are defined by their distance (L) and relative azimuth (γ_0) to the reference collector, as illustrated in Fig. 4. The coordinates of the projected shadow of one collector can then be defined as:

$$x_0 = L \cdot \sin(\gamma - \gamma_0) \tag{1}$$

$$y_0 = -L \cdot \cos(\gamma - \gamma_0) \cdot \sin(\alpha) \tag{2}$$

It can be noted that the shadow projection is independent of the collector aperture geometry and tracker height (assuming all trackers have the same height).

2.3.2. Selection of possible shading collectors

The second step is to determine which collectors should be included when calculating the shaded area. Collectors that do not shade the reference collector for the specific time step should not be included for computational reasons.

The most basic selection criterion is to only consider collectors within ± 90° of the reference collector azimuth (i.e., collectors positioned in front of the reference collector). This criterion can be implemented by only considering collectors for which $\cos(\gamma - \gamma_0) > 0$.

The second criterion is based on the distance of the projected shadows relative to the reference collector. In order for the projected shadow and the reference collector to intersect, their bounding circles have to overlap. Therefore, only collectors whose projected shadow coordinate is within a distance equal to the bounding circle diameter D_{min} are considered (illustrated in Fig. 6). Based on the projected shadow center coordinate, the condition can be expressed as:

$$\sqrt{x_0^2 + y_0^2} < D_{min} \tag{3}$$

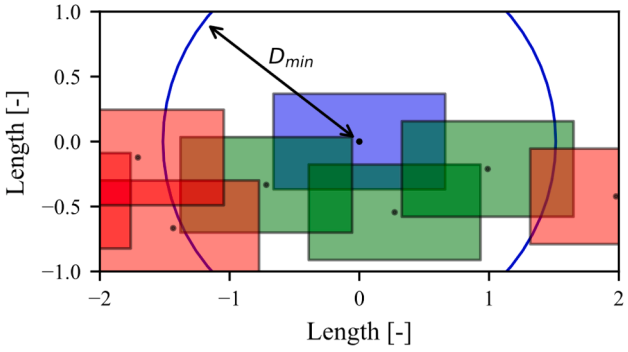

Fig. 6. Selection of possible shading collectors based on the shadow projections relative to the reference collector (blue). The green collectors are selected as shading collectors, whereas the red collectors are disregarded from further calculations for this time step.

2.3.3. Calculation of shading area and fraction

The final step is to calculate the shaded and unshaded area of the reference collector. The method iteratively takes into account the shading effect of the selected collectors. First, the unshaded area is initialized equal to the reference collector geometry. Then, the intersecting area of the shading collector's shadow projection and the unshaded geometry is calculated and subtracted from the unshaded geometry. This step is repeated for all of the possible shading collectors. The calculation of the intersecting area is done analytically using the Python library Shapely, which relies on the GEOS geometry engine (GEOS contributors, 2021).

The fraction of shaded area, called the shading fraction (SF), can then be calculated as:

$$SF = A_{sh}/A_{col} \tag{4}$$

where A_{sh} is the shaded area. The shaded area is equal to the collector area minus the unshaded area.

2.3.4. Implementation and computation time

The shading calculation method has been implemented using the Python programming language. The implementation relies on existing Python packages to take advantage of user familiarity and efficiency in performing their specific tasks. Specifically, the geometric operations, including geometry definition and calculation of the intersecting areas, were handled using the Shapely Python package (Gillies et al., 2007). Calculation of the sun position was carried out using pvlib-python (Holmgren et al., 2018). The code documentation for the shading calculation method and field generation is made available at https://twoaxistracking.readthedocs.io. Version 0.1.0 has been used for the simulations in this study.

An essential prerequisite for shading calculation methods is fast execution, as many iterations have to be performed. For example, for an annual simulation using 15-min data, the shading fraction must be calculated 17,520 times.

To give potential users an idea of the computation time, the annual shading loss was calculated for the case found in Meller (2010). The case consists of circular collectors arranged in a square field layout with a GCR = 0.784. It uses the 15-min Barstow irradiance dataset from 1976. The total simulation time was 12.4 s, executed on a single core of an Intel Core i7 9700 processor. The execution time was comparable to that reported by Meller (2010), though a direct comparison was not possible as they were not run on the same system. Most scenarios would complete in much shorter times as computation time decreases with decreasing GCR.

2.3.5. Assumptions and limitations

The shading calculation method assumes that the collector area is 100% active, meaning there is no part of the collector surface that contributes to shading but not generation. Furthermore, it should be noted that the geometrical shadow projection calculations assume that all trackers are installed on an even field. Also, the method does not account for any potential horizon shading caused by obstructions such as trees or hills. The shading effects of hills or nearby obstructions could be simulated by setting the shading fraction to 1 for a given range of solar azimuths and zenith angles, though this is out of the scope of this study.

Furthermore, due to the relatively high cost of two-axis trackers, they are generally restricted to concentrating solar technologies which require accurate alignment. As only direct irradiance is concentrated, diffuse irradiance is not considered in this study. For modeling the impact of the shading of diffuse radiation (view obstructions), the reader is referred to Deline et al. (2013) and Tschopp et al. (2022).

2.4. Annual shading loss

When considering shading, the shading values must be weighted by irradiation, as otherwise, periods with high shading and low irradiation will skew the results. The simulation results are therefore presented in terms of the annual shading loss (ASL). The ASL is the fraction of annual energy lost due to shading relative to the incident energy when no shading occurs (an infinitely large collector field, GCR = 0):

$$ASL = \frac{\sum_{t=1}^{T} DNI(t) \cdot SF(t)}{\sum_{t=1}^{T} DNI(t)} \tag{5}$$

where T is the number of time-steps (t), $SF(t)$ is the shading fraction and $DNI(t)$ is the direct normal irradiance at time-step t.

2.5. Locations and irradiance data

The numerical layout simulations described in Section 2.2.1 were carried out for four different locations to elucidate the impact of latitude and climate. The locations and the annual DNI are shown in Table 2, ranging from 0 to 55° N latitude.

To allow for comparison to previous studies, Barstow was chosen as one of the locations. Nakuru and Lendemarke were selected to cover a wide range of latitudes. To investigate the role of irradiance level, Tanger was chosen, as it has a similar latitude to Barstow but receives significantly less direct irradiance.

For Barstow, the commonly used 1976 Barstow dataset (described in Section 1) was used to calculate the ASL. The dataset contains a large share of erroneous measurements (periods of unfeasibly high irradiance values, bad tracking, irradiance at night, etc.). To reduce the influence of bad data, the entire dataset was manually quality controlled for erroneous measurements, which were subsequently removed from the analysis. For Nakuru, Tanger, and Lendemarke, 15-min satellite-derived irradiance data was obtained for 2019 from the CAMS Radiation Service (Qu et al., 2016). Satellite-derived irradiance was chosen over ground measurements, as ground-measured irradiance is affected by local horizon obstructions and often has missing data.

2.6. Reference scenario

A reference scenario was defined and will be extensively referred to throughout this paper. The reference scenario consists of the rectangular collector aperture in a square field layout with a GCR of 0.25 and a neighbor order of 2. Additionally, the irradiance data for Lendemarke will be used for the reference scenario. The field parameters correspond roughly to the solar collector field in Lendemarke; hence, the configuration represents realistic conditions. Figs. 3-6 are all based on the reference scenario field layout and aperture shape and represent the shading conditions for a solar azimuth of 210° and solar elevation of 7°.

3. Results and discussion

This section presents the results from the numerical shading simulations. First, the modeling approach is validated in Section 3.1, followed by examples of detailed outputs in Section 3.2. In Section 3.3, the optimal field layouts for each location, aperture shape, and GCR are given, and the results are discussed. The influence of field layout

Table 2
Latitude and annual DNI for the four simulated locations.

Location	Latitude	Annual DNI [kWh/m^2]
Nakuru, Kenya	0.3° N	1942
Barstow, California	34.9° N	2627
Tanger, Morocco	35.8° N	2209
Lendemarke, Denmark	55.0° N	974

parameters is further analyzed in Section 3.4. Finally, the increase in shading for rectangular field layouts is compared to optimum layouts in Section 3.5.

3.1. Validation

In this study, the entire shading modeling approach, from field layout generation to shading calculation, has been validated by replicating the shading calculations for the optimal field layouts in Cumpston and Pye (2014). The reference study used the 1976 Barstow irradiation data, circular collector apertures and only considered time steps for which the solar elevation angle was greater than 10°.

The annual shading loss calculated with the method described in Section 3 (ASL_{calc}) is compared to the results from the reference study (ASL_{ref}) in Table 3. It is apparent that the two methods result in almost identical annual shading losses. The minor differences are most likely due to different pre-processing of the irradiance data (described in Section 2.5).

3.2. Calculated shading outputs

Determining the annual shading losses involves calculating the shading fraction for each time step. However, comparing field layouts at such a level of detail is impractical and not useful for decision-making. It is often sufficient to compare field layouts in terms of the annual irradiation loss (e.g., ASL), though aggregating the shading values comes at the expense of losing daily and seasonal information.

To illustrate the seasonal variation in shading, the daily average shading fraction (unweighted) is shown for the reference case for a square and a rectangular field layout in Fig. 7. The daily average shading fractions in Fig. 7 vary significantly over the year, mainly due to Lendemarke's relatively high latitude, where the sun position experiences large seasonal variations.

Additionally, it can be noted that the square and rectangular field layouts are optimal for different parts of the year. For this location, the rectangular layout is shaded the least during the summer months, whereas the square field layout is advantageous during spring and fall. The strong variation in shading over the year and the seasonal preference in layouts illustrate the importance of weighing the shading fraction with irradiation data when calculating the annual shading loss.

Another way to visualize the shading fraction is by using heatmaps, as shown in Fig. 8. The plot represents the shading fraction as a function of solar elevation and azimuth. The plot is essentially a visual representation of a look-up table, which can be used for simulation programs (where the shading fraction is pre-calculated for all possible solar positions). The program can then simply look up the shading fraction based on the solar position at the time step, interpolating between values if necessary. Contrary to the shading simulations carried out in this study, a specific solar angle step size has to be chosen when generating a look-up table. In Fig. 8, for example, a step size of 1° was used. For multi-year or multi-site simulations of the same field layout and aperture, this method results in fewer shading calculations as the values in the look-up table can be reused. As an example, the sun path lines for the 21st of March, June, and December are shown for Lendemarke in Fig. 8.

Table 3
Comparison of the annual shading loss from the reference study (ref) and calculated by the method described in this paper for various GCRs.

GCR	ASL_{ref} [%]	ASL [%]	ASL_{diff} [%]
0.2	1.53	1.53	0.00
0.3	4.50	4.53	−0.03
0.4	8.14	8.13	0.01
0.5	12.4	12.3	0.10
0.6	17.2	17.1	0.10
0.7	22.3	22.2	0.10
0.8	27.6	27.4	0.20
0.9	33.1	32.9	0.20

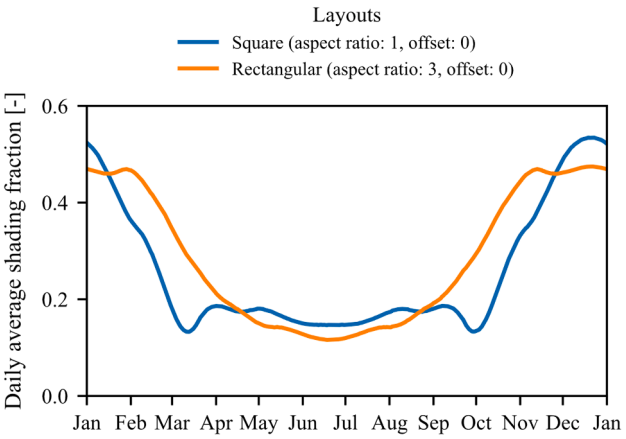

Fig. 7. Daily average shading fraction for a square and rectangular field layouts based on the reference scenario (Lendemarke, GCR = 0.25). The rotation for both layouts is zero.

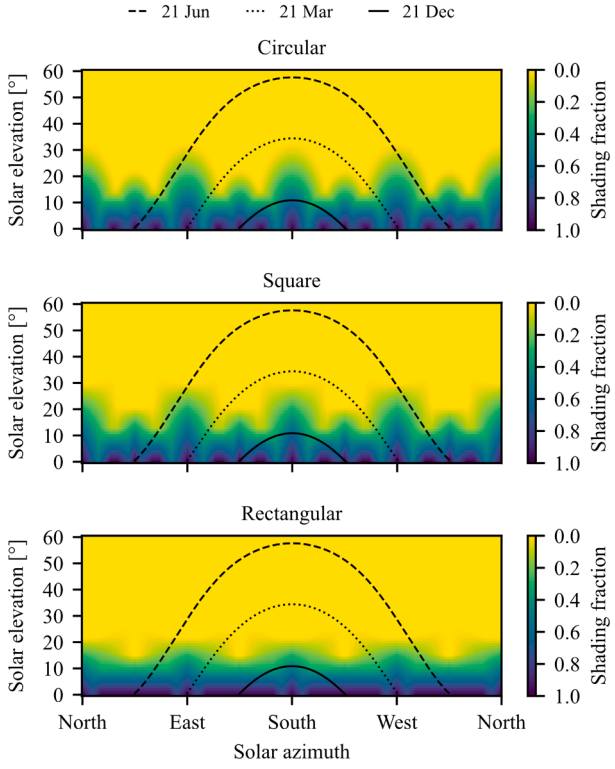

Fig. 8. 2D visualization of the shading fraction as a function of solar elevation and azimuth for three different collector apertures arranged in a square field layout with GCR = 0.25. The sun path lines correspond to Lendemarke, Denmark.

Since the results in Fig. 8 are based on a square field layout (reference scenario), they are symmetric around the north-south and east-west axis and the diagonals. The figure also shows the maximum solar elevations at which collectors in the cardinal and ordinal directions cause shading. Furthermore, as all three collector apertures are shown in Fig. 8, they are useful for comparing the different shading conditions, as discussed in the following section.

3.3. Optimum field layouts

This section presents the optimum field layouts from the numerical

shading investigation of the four locations and three aperture shapes for the discretized field layouts (described in Section 2.2.1). The optimum field layouts and corresponding ASLs for a representative range of GCRs are listed in Table 4. As expected, the shading losses strictly increase with increasing GCR, ranging from negligible levels of shading to annual losses of more than 18%.

When comparing the different locations, the shading losses generally increase with increasing distance from the equator. The higher shading losses are mainly due to the lower average sun elevation at sites further from the equator. Consequently, the economical optimum GCR for a solar plant will decrease with increasing latitude, assuming fixed land costs.

When looking at the aspect ratios in Table 4, it is evident that there is a trend of decreasing aspect ratios with increasing GCR. The decrease in optimum aspect ratios can partly be explained by the fact that the maximum feasible aspect ratio also decreases with increasing GCR. For the northernmost location (Lendemarke), the optimum aspect ratio does not differ considerably, ranging from 1.25 to 0.87. A more squarish configuration (aspect ratio close to 1) is preferred at Lendemarke because the sun extends much further east and west, which causes the incoming irradiation from the east and west to be comparable to that from the south. The opposite trend is true near the equator, where the optimum aspect ratio for Nakuru is equal to the maximum for GCR $>$ 0.2.

Concerning aperture shape, there is not a significant difference in shading losses at low GCRs. However, for more compact field layouts, the choice of aperture shape significantly influences shading losses by up to 2.7%. As shown in Table 4, the rectangular aperture was the most favorable for all cases, with the square aperture being the least. The influence of aperture shape is also latitude dependent and becomes more pronounced for locations further away from the equator.

Part of the explanation for the reduced shading losses for the rectangular aperture can be found in the shading fraction plots in Fig. 8. The heatmaps show that significant shading occurs up to a solar elevation of $\sim 30^\circ$ for the circular and square apertures. Contrastingly, for the rectangular aperture, shading only occurs up to $\sim 20^\circ$ solar elevation. Consequently, the shading fraction below 20° solar elevation for the rectangular aperture is greater on average than the other two apertures. However, irradiance is often higher at larger solar elevations due to the lower air mass; thus, the rectangular aperture's distribution of shading factor vs. solar elevation is advantageous.

Unlike Cumpston and Pye (2014), who found that above a certain GCR, diamond layouts (offset $= \pm 0.5$) and hexagonal layouts (aspect ratio $= \sqrt{3}/2$) were more favorable than rectangular field layouts, such a trend was not found in this study. The difference in results can be attributed to Cumpston and Pye (2014), not including periods where the solar elevation was below 10°, as simulations excluding irradiance below 10° proved identical results. This study considered all periods as many modern-day trackers are not limited in their rotation, and since shading mainly occurs below 10° solar elevation. This finding demonstrates that the arbitrary threshold of 10° influences the results.

3.4. Influence of field layout parameters

The information presented in Table 4 is the condensed result of millions of simulated field layouts. To delve deeper into the data, the ASL as a function of the layout parameters is shown in Fig. 9 for the rectangular aperture. Each subplot is a contour plot of the ASL, where for each combination of aspect ratio and offset, the optimum rotation has been chosen. The optimum configuration for each GCR and location is marked by a red dot. As previously noted, Fig. 9 also shows that the optimum aspect ratio decreases with increasing latitude for all of the locations.

When comparing Tanger and Barstow, which have similar latitudes, Fig. 9 shows that they are similarly affected by the field layout parameters, i.e., the shading contours are similar. For GCRs 0.2 and 0.3, the optimum configurations are essentially identical, and there is only a small difference in the optimum layout for GCR $= 0.1$. However, there is

Table 4
Optimum field layouts for scenarios defined by location, aperture shape, and GCR. Cells marked by a dash correspond to non-feasible layouts.

		Circular				Square				Rectangular			
	GCR	Aspect ratio	Offset	Rotation	ASL	Aspect ratio	Offset	Rotation	ASL	Aspect ratio	Offset	Rotation	ASL
Nakuru	0.10	6.20	−0.50	175°	0.1	3.90	−0.50	160°	0.1	2.80	−0.50	160°	0.1
	0.20	2.60	−0.50	160°	0.7	2.20	−0.50	155°	0.8	2.05	0.05	0°	0.7
	0.25	2.70	−0.50	0°	1.2	2.00	−0.50	160°	1.5	1.65	−0.25	0°	1.2
	0.30	2.25	−0.50	0°	1.9	1.67	−0.50	165°	2.3	1.39	−0.50	0°	1.8
	0.40	1.70	−0.00	0°	3.5	1.25	−0.35	160°	4.3	1.05	0.50	0°	3.4
	0.50	1.40	−0.10	0°	5.8	1.00	−0.35	160°	6.7	–	–	–	–
Barstow	0.10	2.15	−0.50	160°	0.9	1.85	−0.50	155°	1.0	2.70	−0.50	170°	0.8
	0.20	1.05	0.50	25°	3.8	1.20	0.50	20°	4.0	1.55	0.15	0°	3.0
	0.25	1.35	−0.50	175°	5.6	1.25	−0.50	170°	5.9	1.35	0.00	0°	4.5
	0.30	1.20	−0.50	175°	7.4	1.15	−0.50	175°	7.8	1.10	0.50	25°	6.0
	0.40	0.95	−0.50	0°	11.3	0.95	−0.50	0°	12.0	0.90	−0.45	150°	9.3
	0.50	0.87	0.50	0°	15.5	0.87	−0.50	0°	16.6	–	–	–	–
Tanger	0.10	2.00	−0.50	160°	0.7	2.00	−0.50	160°	0.8	2.00	−0.5	160°	0.6
	0.20	1.50	−0.50	165°	3.0	1.30	−0.50	165°	3.3	1.55	0.15	0°	2.4
	0.25	1.25	−0.50	170°	4.7	1.20	−0.50	170°	4.9	1.35	0.50	5°	3.6
	0.30	1.10	−0.50	175°	6.3	1.05	−0.50	175°	6.7	1.10	0.50	25°	4.9
	0.40	0.90	−0.45	175°	9.8	0.90	−0.45	175°	10.5	0.90	0.45	30°	8.0
Lendemarke	0.50	0.87	−0.50	0°	13.9	0.89	−0.45	175°	14.9	–	–	–	–
	0.10	1.20	0.20	35°	1.0	1.20	0.20	35°	1.1	1.25	0.40	30°	0.7
	0.20	1.20	0.05	40°	3.7	1.20	0.05	40°	3.9	1.10	0.25	35°	2.9
	0.25	1.10	−0.05	45°	5.5	1.10	−0.05	45°	5.8	1.05	0.30	35°	4.5
	0.30	1.10	−0.10	45°	7.7	1.05	−0.05	45°	8.1	1.00	0.35	35°	6.3
	0.40	1.00	−0.20	50°	12.6	1.00	0.05	130°	13.2	0.90	0.45	30°	10.5
	0.50	0.87	0.50	0°	18.1	0.95	0.50	55°	18.8	–	–	–	–

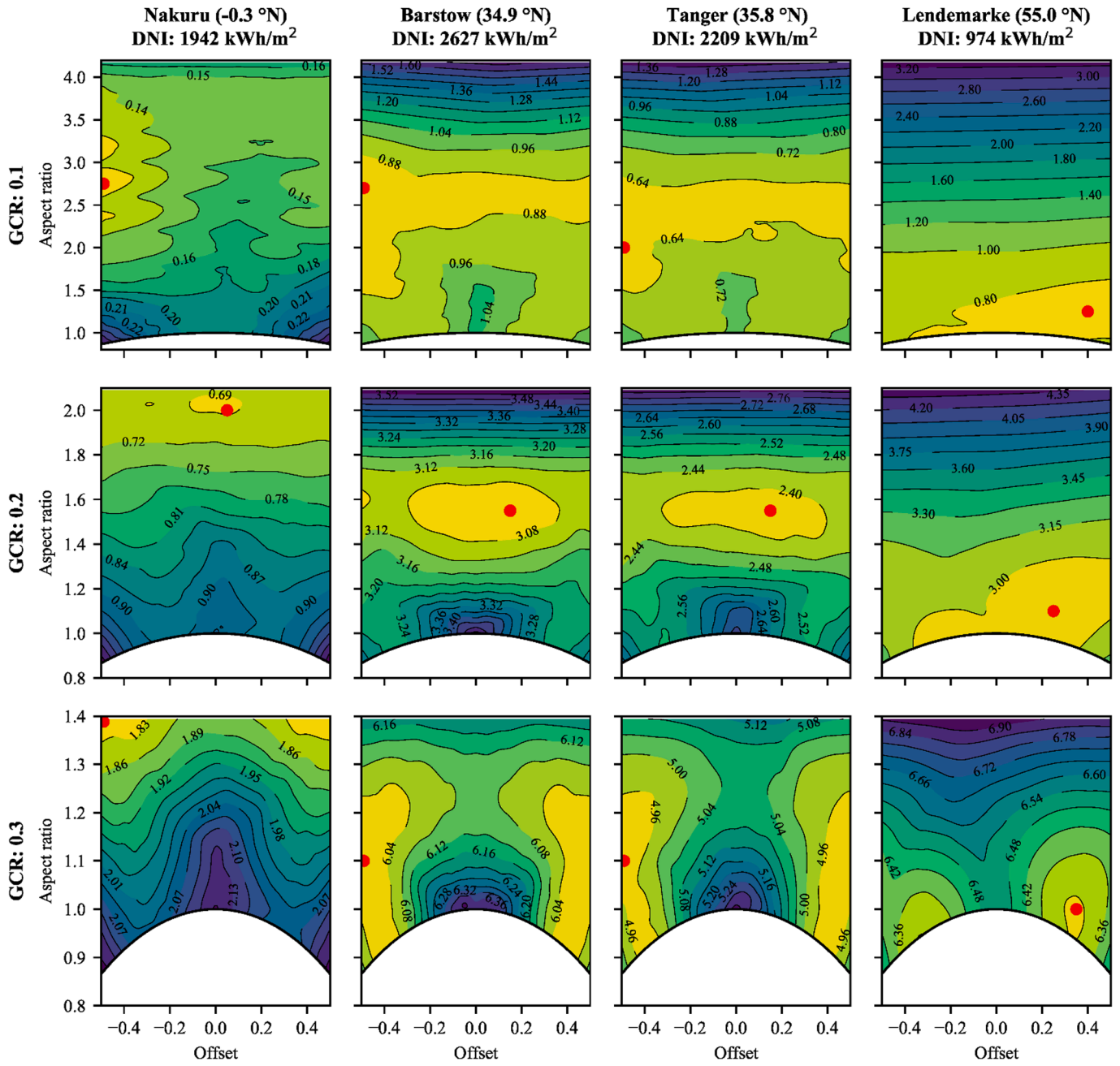

Fig. 9. Contour plots of the annual shading loss in percentage assuming optimal rotation. The results are presented for the rectangular aperture for four different locations and GCRs of 0.1, 0.2, and 0.3. The optimal layout for each location and GCR is marked by a red dot.

a difference in the absolute shading losses: the ASL contour values for Barstow are somewhat higher than for Tanger. This difference could be due to the difference in irradiance, although further research is needed to fully elucidate the impact of irradiance levels on shading, as daily weather patterns might also play a role. Nonetheless, it indicates that the local climate can have an impact on shading losses.

While choosing a favorable combination of aspect ratio and offset can reduce shading, GCR is the dominant parameter determining the amount of shading for a specific location. Particularly, the influence of layout parameters becomes smaller with increasing GCR, as the parameter space of feasible layouts decreases. Nevertheless, the variations in ASL are higher for the more northern locations, indicating that the choice of field layout becomes more important with increasing latitude.

As the results presented in Fig. 9 were for the rectangular collectors, the findings may not be valid for other aperture shapes. To investigate this, contour plots for all three investigated aperture shapes are presented in Fig. 10. In this figure, it can be clearly seen that the optimum field layouts and contour lines for the circular and square apertures are very similar. In contrast, a zero offset is favored for the rectangular aperture, and the contours differ from the other two apertures. Therefore, it can be expected that design rules from studies on circular apertures can be applied to square collectors but not necessarily to rectangular collectors.

Based on Fig. 9 and Fig. 10, it seems that the optimization surfaces are amenable to gradient-based optimization methods. Therefore, if only the optimal layout is of interest, it may be determined quicker using gradient descent algorithms rather than investigating the entire design space.

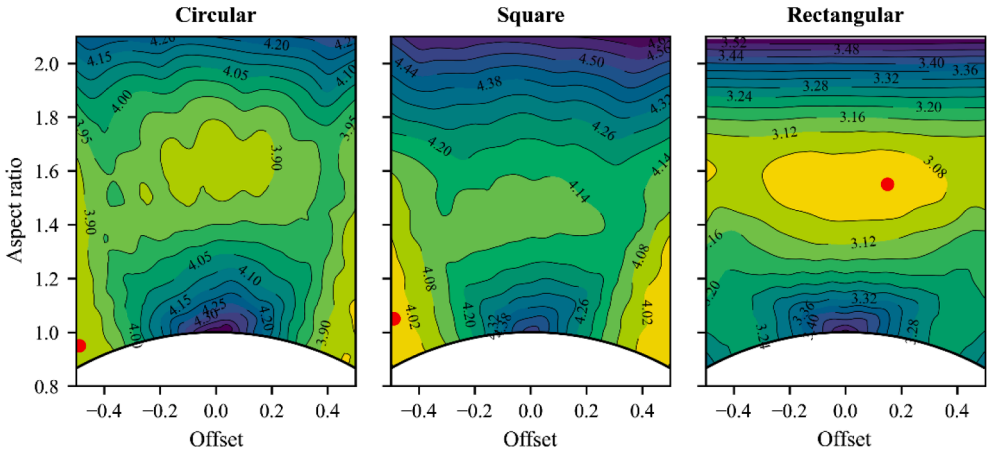

Fig. 10. Shading fraction as a function of aspect ratio and offset for the three aperture geometries. Simulations are for Barstow using a GCR of 0.2.

3.5. *Rectangular field layouts*

While very few of the optimum field layouts found in Table 4 are rectangular (offset = 0), in practice, most two-axis trackers are arranged in rectangular layouts. This is primarily due to practical and economic reasons, e.g., piping and wiring. An example of the increase in shading losses due to choosing a rectangular layout compared to the optimum field layout is shown in Fig. 11.

Fig. 11 shows that for optimally rotated rectangular layouts, the increase in shading losses is practically negligible for GCR $<$ 0.25. Additionally, the non-rotated field layouts for the three southern locations are the same as the optimally rotated, whereas the optimally rotated field layouts in Lendemarke result in a shading loss reduction up to 0.5%. For closely packed fields (GCR $>$ 0.3), the increase in shading losses due to choosing a rectangular layout starts to become significant, which was also seen for circular and square apertures (not visualized for space-saving reasons).

However, choosing a particular rotation is not always possible (as assumed in Fig. 9 and Fig. 10). In reality, the field rotation is often restricted by the shape of the available plot of land. It is, therefore, interesting to investigate the impact of sub-optimal rotation for rectangular field layouts, as shown in Fig. 12. This figure shows the annual

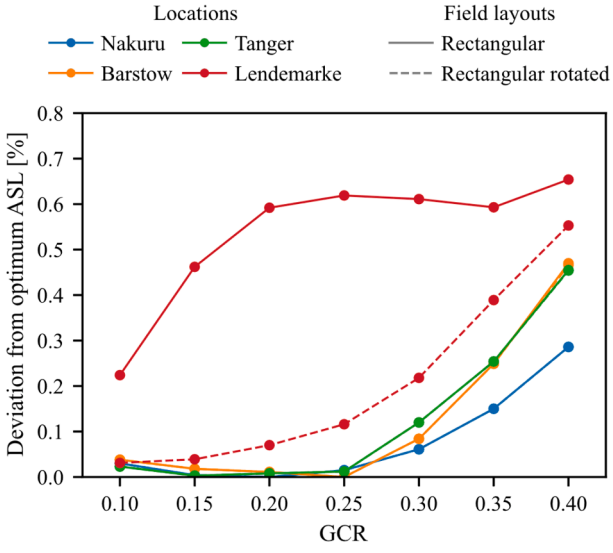

Fig. 11. Increase in shading losses for different layouts as a function of GCR for the rectangular aperture. The layouts denoted as "rectangular" have a rotation = 0, whereas, for the rectangular rotated layouts, the optimal rotation has been chosen.

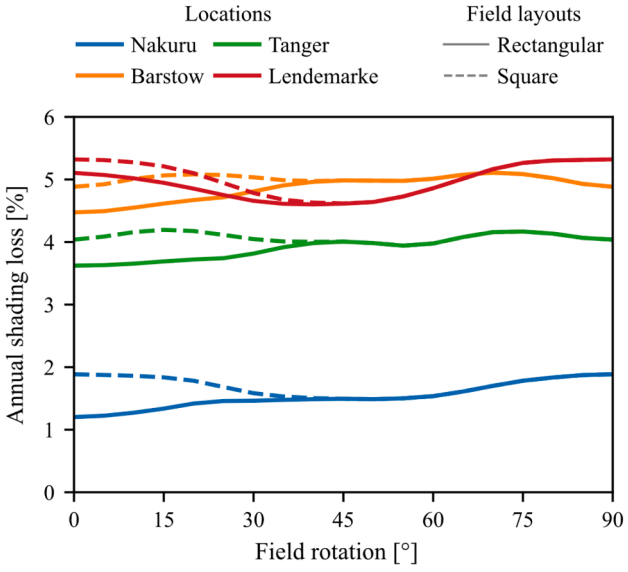

Fig. 12. Impact of field rotation on shading losses for square (dashed) and rectangular (solid) field layouts. Results are based on the rectangular aperture and GCR = 0.25. The rectangular field layout is identical to the square layout for rotations $>$ 45°. The graph only shows simulations where field rotation $\leq$ 90° due to the symmetry of rectangular layouts.

shading loss for square and rectangular field layouts as a function of field rotation.

For the rectangular field layouts, the increase in shading losses due to sub-optimal rotation is between 0.64 and 0.72% for all locations. For solar energy system designers, this means that a noticeable energy gain can be achieved by choosing a plot of land with a favorable orientation. Also, there is significant energy gain for Nakuru, Tanger, and Barstow by choosing a rectangular layout over a square layout, whereas the difference is minor for Lendemarke.

4. Conclusion

A method suitable for calculating self-shading of two-axis tracking collectors of arbitrary geometry was demonstrated and validated by comparison to previous work. The method was implemented in Python and has been made freely available. Subsequently, the method was used to perform a numerical investigation of the annual shading loss for different field layouts for three aperture shapes and four locations.

It was shown that the optimum aspect ratio decreases with increasing

distance from the equator, implying a preference for more squarish field layouts at northern locations. Similarly, shading losses increase with increasing latitude; hence it is expected that the economical optimum plant layout is closer packed (higher GCR) closer to the equator, assuming similar land costs.

Results showed that the shading losses were lowest for the rectangular collector aperture and highest for the square aperture. While the technology type generally dictates the general aperture shape (e.g., circular or rectangular/square), the relatively large difference in shading losses between the square and rectangular aperture indicates potential in optimizing the solar collector design to minimize shading losses.

Additionally, the impact of the field layout parameters on shading was investigated, and it was found that circular and square apertures were similarly affected. Therefore, general design rules from studies on circular collectors are expected to be transferrable to square collectors but not necessarily to rectangular collectors.

Declaration of Competing Interest

The authors declare that they have no known competing financial interests or personal relationships that could have appeared to influence the work reported in this paper.

Acknowledgments

This work was supported by the Danish Energy Agency under the Energy Technology Development and Demonstration Program (EUDP) [grant number 64018-0606].

Data availability

The source code documentation for the shading calculation method and notebooks for reproducing the numerical simulations are available at https://twoaxistracking.readthedocs.io.

References

Apley, W.J., 1979. SHADE - A computer model for evaluating the optical performance of two-axis tracking parabolic concentrators. In: American Society of Mechanical Engineers (Paper), pp. 1–7.

Cumpston, J., Pye, J., 2014. Shading and land use in regularly-spaced sun-tracking collectors. Sol. Energy 108, 199–209. https://doi.org/10.1016/j.solener.2014.06.012.

Deline, C., Dobos, A., Janzou, S., Meydbray, J., Donovan, M., 2013. A simplified model of uniform shading in large photovoltaic arrays. Sol. Energy 96, 274–282. https://doi.org/10.1016/j.solener.2013.07.008.

Díaz-Dorado, E., Cidrás, J., Carrillo, C., 2017. A method to estimate the energy production of photovoltaic trackers under shading conditions. Energy Convers. Manag. 150, 433–450. https://doi.org/10.1016/j.enconman.2017.08.022.

Dobos, A.P., 2014. PVWatts Version 5 Manual. National Renewable Energy Laboratory, Golden, CO. https://doi.org/10.2172/1158421.

Duffie, J.A., Beckman, W.A., Blair, N., 2020. Solar Engineering of Thermal Processes, Photovoltaics and Wind, 5th ed. John Wiley & Sons. https://doi.org/10.1002/9781119540328.

Elayeb, M.E., Haman, R.A., Siala, F.M.F., 2014. Calculation of the blocking factor in heliostat fields. Energy Proc. 57, 291–300. https://doi.org/10.1016/j.egypro.2014.10.034.

Fartaria, T.O., Pereira, M.C., 2013. Simulation and computation of shadow losses of direct normal, diffuse solar radiation and albedo in a photovoltaic field with multiple 2-axis trackers using ray tracing methods. Sol. Energy 91, 93–101. https://doi.org/10.1016/j.solener.2013.02.008.

GEOS contributors, 2021. GEOS coordinate transformation software library. https://libgeos.org/.

Gillies, et al., 2007. Shapely: manipulation and analysis of geometric objects.

Gilman, P., Dobos, A., DiOrio, N., Freeman, J., Janzou, S., Ryberg, D., 2017. SAM Photovoltaic Model Technical Reference Update.

Gordon, J.M., Wenger, H.J., 1991. Central-Station Solar Photovoltaic Systems: sensitivity studies. Sol. Energy 46, 211–217. https://doi.org/10.1016/0038-092X(91)90065-5.

Holmgren, W.F., Hansen, C.W., Mikofski, M.A., 2018. Pvlib Python: a Python Package for Modeling Solar Energy Systems. J. Open Source Softw. 3, 884. https://doi.org/10.21105/joss.00884.

Jensen, A.R., et al., 2022. Thermal performance assessment of the world's first solar thermal Fresnel lens collector field. Sol. Energy. https://doi.org/10.1016/j.solener.2022.01.067.

Klein, S.A. et al., 2017. TRNSYS 18: A Transient System Simulation Program.

Linn, J.K., Zimmerman, J.C., 1979. A Method for Calculating Shadows Cast by Two-Axis Tracking Solar Collectors. SAND-79-0190. https://doi.org/10.2172/5623740.

Meller, Y., 2010. Analytically calculating shading in regular arrays of sun-pointing collectors. Sol. Energy 84 (11), 1967–1974. https://doi.org/10.1016/j.solener.2010.08.006.

Meller, Y., Kribus, A., 2013. Kaleidoscope homogenizers sensitivity to shading. Sol. Energy 88, 204–214. https://doi.org/10.1016/j.solener.2012.11.010.

Narvarte, L., Lorenzo, E., 2008. Tracking and Ground Cover Ratio. Prog. Photovolt Res. Appl. 16 (8), 703–714. https://doi.org/10.1002/pip.847.

Noone, C.J., Torrilhon, M., Mitsos, A., 2012. Heliostat field optimization: A new computationally efficient model and biomimetic layout. Sol. Energy 86 (2), 792–803. https://doi.org/10.1016/j.solener.2011.12.007.

Nsengiyumva, W., Chen, S.G., Hu, L., Chen, X., 2018. Recent advancements and challenges in Solar Tracking Systems (STS): A review. Renew. Sustain. Energy Rev. 81, 250–279. https://doi.org/10.1016/j.rser.2017.06.085.

Osborn, D.B., 1980. Generalized Shading Analysis for Parabolodial Collector Fields. In: Energy Technology Conference & Exhibition, American Society of Mechanical Engineers. pp. 1–8.

Pons, R.L., Dugan, A.F., 1984. The effect of concentrator field layout on the performance of point-focus distributed receiver systems. J. Sol. Energy Eng. Trans. ASME 106, 35–38. https://doi.org/10.1115/1.3267559.

Qu, Z., Oumbe, A., Blanc, P., Espinar, B., Gesell, G., Klüser, L., Lefèvre, M., Saboret, L., Wald, L., Paristech, M., Observation, O.I.E.C., Antipolis, S., 2016. Fast radiative transfer parameterisation for assessing the surface solar irradiance: The Heliosat-4 method. Meteorologische Zeitschrift 26, 33–57. https://doi.org/10.1127/metz/2016/0781.

Tian, Z., Perers, B., Furbo, S., Fan, J., 2018. Thermo-economic optimization of a hybrid solar district heating plant with flat plate collectors and parabolic trough collectors in series. Energy Convers. Manag. 165, 92–101. https://doi.org/10.1016/j.enconman.2018.03.034.

Tschopp, D., Jensen, A.R., Dragsted, J., Ohnewein, P., Furbo, S., 2022. Measurement and modeling of diffuse irradiance masking on tilted planes for solar engineering applications. Sol. Energy 231, 365–378. https://doi.org/10.1016/j.solener.2021.10.083.